# Shear Stress in Epiphyseal Growth Plate is a Risk Factor for Slipped Capital Femoral Epiphysis

*Oskar Zupanc, MD, PhD,* Miran Križančič, MD,* Matej Daniel, PhD,† Blaž Mavčič, MD, PhD,*‡ Vane Antolič, MD, PhD,* Aleš Iglič, PhD,§ and Veronika Kralj-Iglič, PhD‡*

**Background:** Slipping of the capital femoral epiphysis is an important orthopaedic problem of early adolescence. Many hypotheses about its etiology have been examined, yet the underlying mechanisms have not yet been fully elucidated. We examined elevated shear stress in the epiphyseal growth plate and elevated contact hip stress exerted on the femoral head as risk factors for slipping of the capital femoral epiphysis.

**Methods:** Two groups of hips were compared: a group of 100 hips contralateral to the slipped ones and a group of 70 age- and gender-matched healthy hips. The characteristics of individual hips were incorporated by means of geometrical parameters determined from standard anteroposterior radiographs. Shear stress was calculated by using a mathematical model where the femoral neck was considered to function as an elastic rod. Contact hip stress was calculated by the HIPSTRESS method.

**Results:** Hips contralateral to the slipped ones had higher average shear stress (0.81 vs 0.51 MPa; $P < 0.001$) and more vertically inclined physeal angle (55.4 vs 63.2 degrees.; $P < 0.001$) in comparison to healthy hips. Shear stress in the contralateral hips to the slipped ones remained significantly higher even when normalized to the body weight (1400 vs 1060 Pa/N; $P < 0.001$). There was no significant difference in the average contact hip stress (1.86 vs 1.74 MPa; $P = 0.145$).

**Conclusions:** Elevated shear stress, but not elevated contact stress, is a risk factor for slipping of the capital femoral epiphysis.

**Level of evidence:** III (prognostic study, case-control study).

**Key Words:** slipped capital femoral epiphysis, femoral epiphysis, femoral head, epiphyseal plate, growth plate, biomechanics

(*J Pediatr Orthop* 2008;28:444–451)

Slipped capital femoral epiphysis (SCFE) is a disease of the hip occurring during the period of rapid adolescent growth. It is characterized by separation of the epiphysis from the metaphysis of the femoral neck. Endocrine,[1] genetic,[2] and mechanical factors[3–9] contribute to its etiology. However, the underlying mechanisms are not yet completely understood.

The scope of this work is the mechanical factors. The hip load can be described by the resultant hip force, $\boldsymbol{R}$, which is connected to the radial contact stress on the load-bearing surface of the hip,[10–12] and to the shear stress in the femoral neck.[13] The resultant hip force depends on femoral and pelvic geometry.[14] Chung et al[4] experimentally determined that the magnitude of load exerted on the femoral head produces shear stress sufficient to cause an artificial SCFE, indicating that shear stress in the femoral neck may have an important role in the pathogenesis of SCFE. The impact of various factors on the shear stress in the femoral neck was studied.[5,7,9,15] However, to our knowledge, the effect of the shear stress on the clinical status of the patient has not been studied for a large population of patients with SCFE. Previous studies have demonstrated that contact hip stresses play a role in hip pathology.[13,16–18] Therefore, it is of interest to study also the role of the contact hip stress in SCFE.

In our article, the peak shear stress in the epiphyseal growth plate of the hip and the peak contact hip stress, together with underlying biomechanical parameters and geometrical parameters of the hip and pelvis, were determined for hips contralateral to the slipped ones and compared with the respective values obtained in healthy hips. Our analysis was based on assumption that hips contralateral to the slipped ones have the same geometry as the slipped hips had before the slipping and are therefore at increased risk for slipping.[10,19]

## METHODS

Radiographs of 100 patients who were operated on between 1970 and 2005 for unilateral SCFE were selected from the archive of the Department of Orthopaedic Surgery, University Medical Center Ljubljana. The chosen patients had no neurological or musculoskeletal disease. The mean angle of capital femoral slipping on lateral radiographs[20] was 39.7 ± 20.4 (range, 10–80) degrees. According to Southwick[20] and Boyer et al,[21] the slippage was graded as mild in 47 hips, moderate in 16 hips, and severe in 37 hips. It should be noted that only asymptomatic contralateral hips to the slipped ones were included in our study. The records contained standard anteroposterior (A–P) and lateral radiographs of the pelvis and both proximal femora. To rule out possible growth-related changes of the pelvis, only preoperative radiographs taken within 30 days before the operation were included in the study. We also measured posterior slope angles from lateral radiographs of the pelvis and both proximal femora.[3] According to the past and present clinical guidelines of our institution, all

From the *Department of Orthopaedic Surgery, University Medical Center Ljubljana, Ljubljana, Slovenia; †Department of Mechanics, Biomechanics and Mechatronics, Faculty of Mechanical Engineering, Czech Technical University in Prague, Prague, Czech Republic; ‡Laboratory of Clinical Biophysics, Faculty of Medicine; and §Laboratory of Physics, Faculty of Electrical Engineering, University of Ljubljana, Ljubljana, Slovenia.

None of the authors received financial support for this study.

Reprints: Veronika Kralj-Iglič, PhD, Laboratory of Clinical Biophysics, Institute of Biophysics, Faculty of Medicine, University of Ljubljana, Lipičeva 2, SI-1000 Ljubljana, Slovenia. E-mail: veronika.kralj-iglic@fe.uni-lj.si.

patients with unilateral SCFE also undergo preventive fixation in situ with screws on the contralateral (ie, unaffected) side due to the high risk of subsequent bilateral involvement (reported risk as high as 63%[19]). Thus, all contralateral hips to the slipped ones in this study were already preventively fixed in situ, and consequently, no further cases of slipping were observed.

The control group data were obtained from A–P and lateral radiographs of 35 age-matched persons (70 hips) without any evidence of pathological changes in the pelvis and proximal femora. The indication for radiographic examination of these hips was minor leg length discrepancy and pain in the lower back, groin, hip, or gluteal region of unknown origin, where clinical and radiographic examination had shown no skeletal abnormalities. None of the subjects in the control group later developed SCFE or any other intra-articular disease of the hip.

It should be clearly stated that this was a retrospective study of radiographic materials in the archives, without any interventions and without any influence on prospective treatment of included subjects. Only archived radiographs were used, and no physical or radiographic examination was needed or performed for the sole purpose of this study.

The magnitude of the resultant hip force ($R$) and the peak radial contact hip stress ($p_{max}$) were determined by the HIPSTRESS method[22] (for brief explanation of the method, see Appendix 1), consisting of the corresponding mathematical models of the resultant hip force in the one-legged stance[14] and of the contact hip stress.[12] The mathematical model of the resultant hip force is based on the equations of static equilibrium of forces and torques acting on the body segments, whereas the mathematical model of the contact hip stress is based on the assumption that stress in the hip cartilage is proportional to strain. Individual variations in femoral and pelvic geometry (Fig. 1A) were taken into account by rescaling the reference muscle attachment points and the interhip distance.[22] The input parameters of the model for determination of the resultant hip force include geometrical parameters of the hip and pelvis (Fig. 1A): the distance between the centers of the femoral heads, that is, the interhip distance ($l$); the vertical distance between the center of the femoral head and the highest point on the crista iliaca, that is, the pelvic height ($H$); the horizontal distance between the center of the femoral head and the most lateral point on the crista iliaca, that is, the pelvic width ($C$); and the vertical and the horizontal distances from the center of the femoral head to the effective muscle attachment point ($T$) on the greater trochanter ($x$ and $z$, respectively). The point $T$ is determined by the intersection of the contour of the greater trochanter and the normal through the midpoint of the straight line connecting the most lateral point and the highest point on the greater trochanter. To determine the peak radial contact hip stress ($p_{max}$), additional parameters were measured: the Wiberg center-edge angle ($\vartheta_{CE}$)[23] and the radius of the femoral head ($r$).

To determine the peak shear stress in the epiphyseal plate of the femoral neck, the neck was modeled as a beam of circular profile with the diameter $a$ (Fig. 1A) clamped to the femoral diaphysis and subjected to bending and compression. The shear component induces a nonuniform shear stress $\tau$ in the femoral neck with the peak at its center. For a homogenous femoral neck with a circular profile, the peak shear stress in the

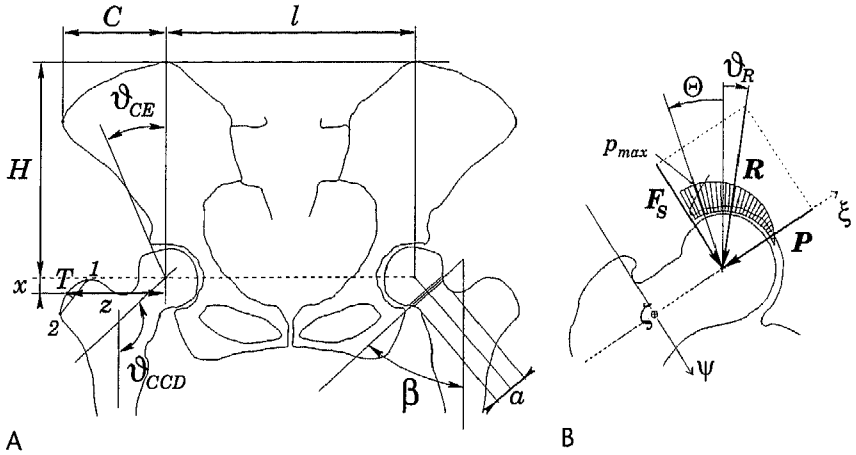


**FIGURE 1.** A, Geometrical and biomechanical input parameters for the HIPSTRESS method: the distance between the centers of the femoral heads $l$, the pelvic height $H$, the width of crista iliaca $C$, and the vertical and the horizontal distances from the center of the femoral head to the effective muscle attachment point $T$ on the greater trochanter ($x$ and $z$, respectively). The point $T$ is determined by the intersection of the contour of the greater trochanter and the normal through the midpoint of the straight line connecting the highest point (1) and the most lateral point (2) on the greater trochanter. To determine the peak radial contact hip stress ($p_{max}$), the Wiberg center-edge angle ($\vartheta_{CE}$) and the radius of the femoral head ($r$) are measured additionally. Estimation of the peak shear stress in the epiphyseal growth plate of the femur also requires measurement of the epiphyseal angle $\beta$, the femoral neck width ($a$), and the neck-to-shaft angle ($\vartheta_{CCD}$). All parameters of a given hip are measured on the same side, but here, they are shown bilaterally for clarity. B, Diagram of the resultant hip force $\boldsymbol{R}$ with vertical inclination angle $\vartheta_R$ and its components $P$ and $F_S$ in the coordinate system of the femoral neck. The contact hip stress distribution and the location of the maximum contact hip stress $p_{max}$ (in the presented case at the pole [$\Theta$]) are also shown.

TABLE 1. The Biomechanical Parameters of Hips at Risk for SCFE (Test Group) and Healthy Hips (Control Group)

| Parameter | Symbol [Units] | Mean SCFE | Mean Control | P (t test) Test/Control | Power (t test) Test/Control |
|---|---|---|---|---|---|
| Body weight | $W_B$ [N] | 590 ± 120 | 500 ± 80 | <0.001* | 0.999 |
| Shear stress | $\tau_{0\beta}$ [MPa] | 0.81 ± 0.25 | 0.51 ± 0.20 | <0.001* | 0.999 |
| Shear stress/$W_B$ (normalized to body weight) | $\tau_{0\beta}/W_B$ [Pa/N] | 1400 ± 370 | 1060 ± 430 | <0.001* | 0.999 |
| Contact hip stress | $p_{max}$ [MPa] | 1.86 ± 0.47 | 1.74 ± 0.52 | 0.145 | 0.313 |
| Contact hip stress/$W_B$ (normalized to body weight) | $p_{max}/W_B$ [Pa/N] | 3210 ± 720 | 3560 ± 1040 | 0.020* | 0.713 |
| Hip joint resultant force | $R$ [N] | 1520 ± 340 | 1320 ± 240 | <0.001* | 0.994 |
| Hip joint resultant force/$W_B$ (normalized to body weight) | $R/W_B$ [1] | 2.59 ± 0.19 | 2.63 ± 0.17 | 0.142 | 0.310 |
| Shear component of $R$ | $F_S$ [N] | 870 ± 230 | 770 ± 160 | 0.001* | 0.913 |
| Shear component of $R/W_B$ (normalized to body weight) | $F_S/W_B$ [1] | 1.48 ± 0.20 | 1.54 ± 0.17 | 0.031* | 0.580 |

*Statistically significant difference.

plane of the epiphyseal cartilage ($\tau_{0\beta}$) can be computed by applying the theory of elasticity (Appendix 2),

$$\tau_{0\beta} = -2R\cos(\vartheta_R + \vartheta_{CCD})\sin(2(\vartheta_{CCD} - \beta))/(\pi a^2) - 16R\sin(\vartheta_R + \vartheta_{CCD})\cos(2(\vartheta_{CCD} - \beta))/(3\pi a^2). \quad (1)$$

All geometrical parameters were determined from A–P radiographs (Fig. 1A). The angle $\beta$ was determined by using the method described by Mirkopulos et al.[7]

All radiographic measurements were performed by a single senior orthopaedic surgeon (O.Z.). Each radiograph was measured once. Body weights ($W_B$) of subjects were obtained from medical records. All biomechanical parameters (the peak shear stress in the epiphyseal growth plate, the peak contact hip stress and the magnitudes of the forces) were calculated both as absolute values ($\tau_{0\beta}$, $p_{max}$, $R$, and $F_S$) and normalized with respect to the body weight ($\tau_{0\beta}/W_B$, $p_{max}/W_B$, $R/W_B$, and $F_S/W_B$). Statistical comparison between the SCFE and the control groups was performed by the unpaired 2-tailed Student $t$ test, and values of $P \leq 0.05$ were considered statistically significant. Power analysis was done for all comparisons of means, and values above 0.80 were considered sufficient. Statistical computations were performed with software programs Microsoft Office Excel 2003 (Microsoft Inc, Redmond, WA) and GPower 2.0 (Faul F. and Erdfelder E., Bonn, Germany).

## RESULTS

The group of contralateral hips to the slipped ones (the SCFE group) consisted of 59 boys and 41 girls, with a mean age of 13.0 ± 1.4 (range, 10.7–16.6) years. The average posterior slope angle[3] in the contralateral hips of the SCFE group was 5.7 ± 3.0 (range 0–10) degrees. The hips in the control group belonged to 22 boys and 13 girls, with a mean age of 13.4 ± 1.6 (range, 10.0–16.6) years. The average posterior slope angle[3] in the control group was 5.6 ± 2.4 (range, 0–9) degrees. There was no statistically significant difference between the SCFE and the control groups with regard to posterior slope angle ($P = 0.839$), percentage of female hips ($P = 0.636$), or age ($P = 0.066$).

TABLE 2. The Geometrical Parameters of the Pelvis and Proximal Femur of Hips at Risk for SCFE (Test Group) and Healthy Hips (Control Group)

| Parameter | Symbol [Units] | Mean SCFE | Mean Control | P (t test) Test/Control | Power (t test) Test/Control |
|---|---|---|---|---|---|
| Angle of inclination of the epiphyseal growth plate of the femur | $\beta$ [°] | 55.4 ± 6.8 | 63.2 ± 6.6 | <0.001* | 1.000 |
| Diameter of the femoral neck | $a$ [mm] | 38.6 ± 3.6 | 37.3 ± 4.0 | 0.027* | 0.617 |
| Length of the femoral neck | $d$ [mm] | 47.7 ± 7.9 | 46.1 ± 6.3 | 0.145 | 0.305 |
| Capitatocolodiaphyseal angle | $\vartheta_{CCD}$ [°] | 137.5 ± 6.5 | 136.4 ± 6.2 | 0.267 | 0.198 |
| Interhip distance | $l$ [mm] | 165.0 ± 13.9 | 160.0 ± 19.7 | 0.093 | 0.435 |
| Pelvic height | $H$ [mm] | 138.9 ± 12.0 | 134.6 ± 11.9 | 0.022* | 0.639 |
| Pelvic width | $C$ [mm] | 53.8 ± 10.7 | 48.7 ± 6.7 | <0.001* | 0.973 |
| Horizontal distance from the center of the femoral head to the effective muscle attachment point (T) on the greater trochanter | $z$ [mm] | 54.4 ± 6.8 | 51.0 ± 8.2 | 0.006* | 0.811 |
| Vertical distance from the center of the femoral head to the effective muscle attachment point (T) on the greater trochanter | $x$ [mm] | 10.2 ± 6.0 | 8.3 ± 6.8 | 0.052* | 0.509 |
| Radius of the femoral head | $r$ [mm] | 22.8 ± 1.7 | 22.7 ± 2.1 | 0.796 | 0.058 |
| Wiberg center-edge angle | $\vartheta_{CE}$ [°] | 34.7 ± 5.3 | 32.2 ± 5.3 | 0.003* | 0.854 |

*Statistically significant difference.

Table 1 shows the differences between the contralateral hips of the SCFE group and the control group in biomechanical parameters: body weight ($W_B$), the peak shear stress ($\tau_{0\beta}$ and $\tau_{0\beta}/W_B$), the peak contact hip stress ($p_{max}$ and $p_{max}/W_B$), the magnitude of the resultant hip joint force ($R$ and $R/W_B$), and the shear component of the resultant hip joint force ($F_S$ and $F_S/W_B$). The mean body weight in the SCFE group was significantly higher than that of the control subjects. Hips contralateral to the slipped ones had higher average shear stress in comparison to healthy hips, and the difference remained statistically significant even when shear stress was normalized to the body weight. Differences in other biomechanical parameters were irrelevant: there was no significant difference in the average contact hip stress, and the magnitude of the resultant hip joint force between the 2 groups was not statistically different after normalization to the body weight. Similarly, the shear component of the resultant hip joint force was on average higher in the SCFE group, but lower after normalization to the body weight.

Comparison of geometrical parameters of both groups was done to better understand the above results. The parameters determined are shown in Table 2, and sample radiographs of normal hips and contralateral unslipped hip are shown in Figures 2 and 3. The decisive risk factor for SCFE due to the increased shear stress is the inclination of the epiphyseal growth plate of the femoral neck $\beta$, which was on the average for 8.9 degrees more vertical in the SCFE group than in the control group. The difference was highly statistically significant ($P < 0.001$). The average diameter of the femoral neck $a$ in the SCFE population was larger, which contributes to lower values of the peak shear stress (Eq. (1)) and therefore diminishes the effect of the inclination of the epiphyseal growth plate. However, this counteracting effect was small.

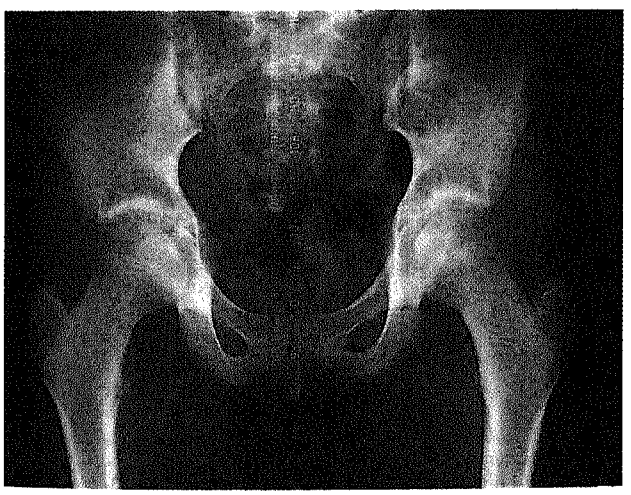

**FIGURE 2.** An anterior-posterior pelvic radiograph of a healthy 13-year-old boy without any signs of hip pathology. The peak shear stress in the epiphyseal growth plate equals 0.40 MPa for the right hip and 0.50 MPa for the left hip. The indication for radiograph was estimation of the leg length discrepancy that later (at skeletal maturity) turned out to be clinically insignificant.

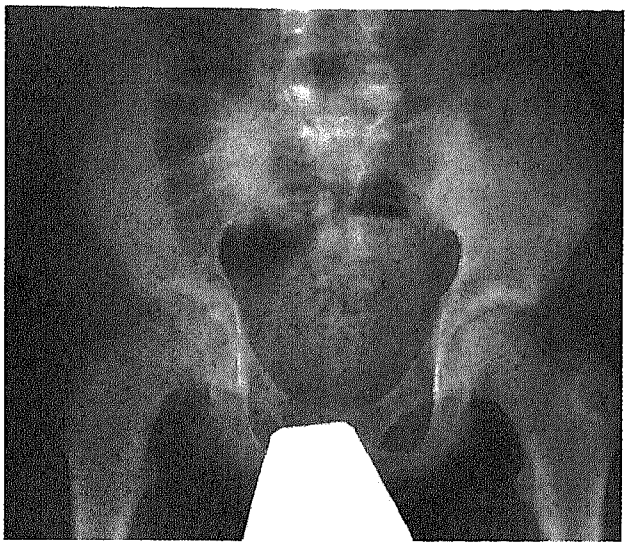

**FIGURE 3.** An anterior-posterior pelvic radiograph of a 13-year-old boy with slipped capital femoral epiphysis of the right hip. The hip on the left was asymptomatic at the time the radiograph was taken, the peak shear stress in its epiphyseal growth plate equals 0.85 MPa. The geometrical features of the left—unslipped—hip include more vertical oriented epiphysis, wider femoral neck for the given head radius, and wider crista iliaca in comparison to the normal hips in Figure 2.

Pelvic height $H$, pelvic width $C$, Wiberg center-edge angle $\vartheta_{CE}$, and horizontal distance from the center of the femoral head to the effective muscle attachment point on the greater trochanter $z$ were larger in the SCFE group than in the control group, whereas the interhip distances and the radii of the femoral heads were not significantly different. The pelvic and femoral shape of the SCFE group therefore contributed to somewhat lower values of the normalized peak contact hip stress when compared with the control subjects, but this effect was counteracted by higher average body weight, and thus, the absolute values of the peak contact hip stress were not significantly different.

## DISCUSSION

We used a mathematical model to estimate the shear stress in the epiphyseal growth plate of the hip for a homogeneous group of hips at risk for SCFE and a group of healthy hips. The components required to assess the shear stress can be determined from the A–P projection, as previously shown.[13] Our results show that the shear stress is higher in the group of hips contralateral to the slipped hips than in the group of healthy hips, the difference (0.81 vs 0.51 MPa) being statistically highly significant ($P < 0.001$). Among the geometrical parameters that determine the shear stress within our model, 2 were most relevant for the difference between the 2 groups: the inclination of the epiphyseal growth plate of the femoral neck $\beta$ and the diameter of the femoral

neck $a$, the effects of the 2 being opposite. However, the effect of the epiphyseal growth plate inclination prevailed.

The importance of the inclination of the epiphyseal growth plate of the femoral neck in adolescents with SCFE was previously reported.[3,5,7,9,24,25] Our results on the inclination of the epiphyseal growth plate of the femoral neck agree with those reported by Speer[9] and Mirkopulos et al,[7] where it was reported that the inclination of the epiphyseal growth plate in the group of nonslipped hips of the SCFE on the average differed from that in the age-matched control by 4.8 degrees ($P < 0.001$)[9] and 4 degrees ($P < 0.001$),[7] respectively. In our study, the difference between the SCFE group and the control group was 8.9 degrees and was statistically highly significant ($P < 0.001$).

Barrios et al[3] have recently found that the posterior slope of the epiphyseal plate with respect to the direction of the femoral neck is a risk factor for SCFE. This is in agreement with the results of Fishkin et al,[5] who found that the retroversion of the femoral neck may increase the shear stress in the femoral neck. Our method uses standard A–P radiographs taken from archives, so the retroversion could not be assessed. However, if available, we could upgrade our method by using radiographs taken in the lateral Lauenstein projection. Because it is expected that taking into account the retroversion would further increase the difference in the shear stress between the hips at risk for SCFE and healthy hips, including the retroversion would not change the conclusions of this work as regarding the shear stress.

Normalized peak contact stress was higher in the group of healthy hips, but this difference was not statistically significant when body weights were also taken into account. One of the main geometrical parameters that contributed to lower normalized contact hip stress in the SCFE group was the Wiberg center-edge angle ($\vartheta_{CE}$) with values 7% greater than in the control group ($P = 0.003$) (34.7 vs 32.2 degrees). This is in agreement with the results of Kitadai et al,[15] who found that the Wiberg center-edge angle was greater in slipped hips than in healthy ones (34.1 vs 32.0 degrees).

Our results show that anatomical features of hips that are at higher risk for SCFE include a wider and higher pelvis, better coverage of the femoral head with pelvic bones, and a thicker femoral neck.

It can be interpreted that on the average, children in the SCFE group had a larger pelvis and femur. This and the observed greater inclination of the epiphyseal growth plate of the femoral neck indicate the growth-related changes due to the influence of some endocrine or biochemical factors on the tissue.[1] In addition, one cannot overlook the significant difference in the body weight between the age- and gender-matched groups of our study, confirming previous findings on the role of body weight in SCFE.[26] It is therefore possible that anatomical changes may be a downstream effect of bone remodeling caused by altered loading during growth and development. This may suggest that the predisposition of the hip to slipping occurs earlier in the patient's lifetime and that targeted radiographic examinations in obese individuals could reveal changes in pelvic geometry even before adolescence. Nevertheless, body weight is a very nonspecific risk factor for SCFE because it is also increasingly common in the general population of adolescents.[27] Estimation of shear stress could therefore offer a valuable additional parameter in targeting subjects at risk.

Based on our results, it can be concluded that increased shear stress in the epiphyseal growth plate of the femoral neck is a risk factor for SCFE independent of the body weight, whereas increased contact hip stress is not. The method presented could be used in adolescents with hip pain of unknown origin for the purpose of early diagnostics, preventive care, and follow-up.

## ACKNOWLEDGMENT

*Computer program HIPSTRESS is available from the authors upon request. The program is free of charge.*

## REFERENCES

1. Wells D, King JD, Roe TF, et al. Review of slipped capital femoral epiphysis associated with endocrine disease. *J Pediatr Orthop.* 1993; 13:610–614.
2. Hägglund G, Hansson LI. Slipped capital femoral epiphysis in three generation. *Acta Orthop Scand.* 1986;57:240–242.
3. Barrios C, Blasco MA, Blasco MC, et al. Posterior sloping angle on the capital femoral physis: a predictor of bilaterality in slipped capital femoral epiphysis. *J Pediatr Orthop.* 2005;25:445–449.
4. Chung SM, Batterman SC, Brighton CT. Shear strength of the human femoral capital epiphyseal plate. *J Bone Joint Surg (Am).* 1976;58-A: 94–103.
5. Fishkin Z, Armstrong DG, Shah H, et al. Proximal femoral physis shear in slipped capital femoral epiphysis—a finite element study. *J Pediatr Orthop.* 2006;26:291–294.
6. Litchman HM, Duffy J. Slipped capital femoral epiphysis: factors affecting shear forces on the epiphyseal plate. *J Pediatr Orthop.* 1984; 4:745–748.
7. Mirkopulos N, Weiner DS, Askew M. The evolving slope of the proximal femoral growth plate relationship to slipped capital femoral epiphysis. *J Pediatr Orthop.* 1988;8:268–273.
8. Pritchett JW, Perdue KD. Mechanical factors in slipped capital femoral epiphysis. *J Pediatr Orthop.* 1988;8:385–388.
9. Speer DP. *Experimental Epiphysiolysis: Etiologic Models of Slipped Capital Femoral Epiphysis. In the hip. Proceedings of the Hip Society.* St Louis: CV Mosby; 1982:68–88.
10. Billing L, Bogren HG, Wallin J. Reliable X-ray diagnosis of slipped capital femoral epiphysis by combining the conventional and a new simplified geometrical method. *Pediat Radiol.* 2002;32:423–430.
11. Brinckmann P, Frobin W, Hierholzer E. Stress on the articular surface of the hip joint in healthy adults and persons with idiopathic osteoarthrosis of the hip joint. *J Biomech.* 1981;14:149–156.
12. Ipavec M, Brand RA, Pedersen DR, et al. Mathematical modelling of stress in the hip during gait. *J Biomech.* 1999;32:1229–1235 and 2002;35:555.
13. Pauwels F. *Biomechanics of the Normal and Diseased Hip.* Berlin: Springer-Verlag; 1976.
14. Iglič A, Srakar F, Antolič V. Influence of the pelvic shape on the biomechanical status of the hip. *Clin Biomech.* 1993;8:223–224.
15. Kitadai HK, Milani C, Nery CAS, et al. Wiberg center angle in patients with slipped capital femoral epiphysis. *J Pediatr Orthop.* 1999;19: 97–105.
16. Hadley NA, Brown TD, Weinstein SL. The effects of contact pressure elevations and aseptic necrosis on the long-term clinical outcome of congenital hip dislocation. *J Orthop Res.* 1990;8:504–513.
17. Mavčič B, Pompe B, Antolič V, et al. Mathematical estimation of stress distribution in normal and dysplastic human hips. *J Orthop Res.* 2002; 20:1025–1030.
18. Maxian TA, Brown TD, Weinstein SL. Chronic stress tolerance levels for human articular cartilage: two nonuniform contact models applied to long term follow-up of CDH. *J Biomech.* 1995;28: 159–166.
19. Jerre R, Billing L, Hansson G, et al. Bilaterality in slipped capital femoral

epiphysis: importance of a reliable radiographic method. *J Pediatr Orthop [B].* 1996;5:80–84.
20. Southwick WO. Osteotomy through lesser trochanter for slipped capital femoral epiphysis. *J Bone Joint Surg (Am).* 1967;49-A:807–835.
21. Boyer DW, Mickelson RM, Ponseti IV. Slipped capital femoral epiphysis: long-term follow-up of 121 patients. *J Bone Joint Surg (Am).* 1981; 63-A:85–95.
22. Iglič A, Kralj-Iglič V, Daniel M, et al. Computer determination of contact stress distribution and the size of the weight-bearing area in the human hip joint. *Comp Meth Biomech Biomed Eng.* 2002;5:185–192.
23. Wiberg G. Studies on dysplastic acetabula and congenital subluxation of the hip joint. *Acta Chir Scand.* 1939;83(Suppl 58):7.
24. Bright RW, Burnstein AH, Elmore SM. Epiphyseal plate cartilage. A biomechanical and histological analysis of failure modes. *J Bone Joint Surg (Am).* 1974;56:688–703.
25. Burrows HJ. Slipped upper femoral epiphysis: characteristics of hundred cases. *J Bone Joint Surg (Br).* 1957;39:641–658.
26. Manoff EM, Banffy MB, Winell JJ. Relationship between body mass index and slipped capital femoral epiphysis. *J Pediatr Orthop.* 2005;25: 744–746.
27. Dostal WF, Andrews JG. A three dimensional biomechanical model of the hip musculature. *J Biomech.* 1981;14:803–812.
28. Johnston RC, Brand RA, Crowninshield RD. Reconstruction of the hip. *J Bone Joint Surg (Am).* 1979;61A:639–652.
29. McLeish RD, Charnley J. Abduction forces in the one-legged stance. *J Biomech.* 1970;3:191–209.
30. Clauser CE, McConville JT, Young JW. Weight, Volume and Centre of Mass of Segments of the Human Body. Aerospace Medical Research Laboratory, Aerospace Medical Division, WPAF Base, OH (USA); 1970.
31. Marghitu DB. *Mechanical Engineers' Handbook.* San Diego, CA: Academic Press; 2001:120–187.

## APPENDIX 1: DETERMINATION OF THE CONTACT HIP STRESS IN THE ONE-LEGGED STANCE BY THE HIPSTRESS METHOD

The origin of the Cartesian coordinate system is chosen in the femoral head center of the loaded leg so that $x$ and $z$ axes lie in the frontal plane, whereas $y$ axis points in the posterior direction. Two segments are distinguished: the loaded leg (the first segment) and the rest of the body (the second segment). The loaded leg bears, which bears the weight $\mathbf{W}_B - \mathbf{W}_L$, where $\mathbf{W}_B$ is the body weight and $\mathbf{W}_L$ is the weight of the loaded leg. The forces and the torques equilibrium conditions for the second segment are

$$\sum_i \mathbf{F}_i - \mathbf{R} + (\mathbf{W}_B - \mathbf{W}_L) = 0, \qquad \text{(A1.1)}$$

$$\sum_i (\mathbf{r}_i \times \mathbf{F}_i) + \mathbf{a}_W \times (\mathbf{W}_B - \mathbf{W}_L) = 0, \qquad \text{(A1.2)}$$

where $\mathbf{a}_W = (0,0,a_W)$ is the moment arm of the force $\mathbf{W}_B - \mathbf{W}_L$, and $\mathbf{r}_i$ is the radius vector to the point of attachment of the $i$-th muscle force ($\mathbf{F}_i$) on the pelvis. Some of the muscles are attached in a rather large area; therefore, they are divided into "effective" muscles. The model includes 9 effective muscles, which are active in the one-legged stance.[14] These muscles are classified in 3 groups according to their positions: anterior (gluteus medius-anterior, gluteus minimus-anterior, tensor fasciae latae, rectus femoris), middle (gluteus medius-middle, gluteus minimus-middle), and posterior (gluteus medius-posterior, gluteus minimus-posterior, piriformis). Each muscle is considered to act along a straight line connecting the point of attachment on the pelvis (given by $\mathbf{r}_i$) and the point of attachment on the femur (determined by the radius vector $\mathbf{r}_i'$). The reference 3-dimensional coordinates of the radius vectors $\mathbf{r}_i$ and $\mathbf{r}_i'$ are taken from Dostal and Andrews.[27] The rotation of the pelvis and of the femur in the frontal plane around $y$-axis is taken into account by using the corresponding rotation matrixes.[14] The force of each individual muscle included in the model is approximated by[14]

$$\mathbf{F}_i = \delta_i A_i \mathbf{e}_i \qquad \text{(A1.3)}$$

where $A_i$ is the relative cross-sectional area of the $i$-th muscle determined from Johnston et al,[28] $\delta_i$ is the average tension in the $i$-th muscle, and $\mathbf{e}_i = (e_{ix}, e_{iy}, e_{iz})$ is the unit vector in the direction of the force of the $i$-th muscle, $i = 1,2,\ldots,9$,

$$\mathbf{e}_i = (\mathbf{r}_i' - \mathbf{r}_i)/|\mathbf{r}_i' - \mathbf{r}_i|. \qquad \text{(A1.4)}$$

The magnitude of the moment arm of the force $\mathbf{W}_B - \mathbf{W}_L$ is determined from the $y$-component of the moment equilibrium equations for the first and the second body segment

$$-W_B c + W_L b - M_y = 0, \qquad \text{(A1.5)}$$

$$(W_B - W_L)a_W + M_y = 0, \qquad \text{(A1.6)}$$

where $a_W$ is the $z$-coordinate of the moment arm $\mathbf{a}_W$, $c$ is the $z$-coordinate of the moment arm of the ground reaction force $\mathbf{W}_B$, $b$ is the moment arm of the weight of the loaded leg $\mathbf{W}_L$ and $M_y$ is the $z$-component of the intersegmental moment $\mathbf{M} = \sum_i (\mathbf{r}_i \times \mathbf{F}_i)$. It follows from Eqs. (A1.5) and (A1.6) that[29]

$$a_W = (W_B c - W_L b)/(W_B - W_L). \qquad \text{(A1.7)}$$

The moment arms $b$ and $c$ are expressed by the interhip distance $l$, $b = 0.24l$, $c = 0.5l$[29], whereas the weight of the leg is approximated by $W_L = 0.16\ W_B$.[30]

The system (A1.1–A1.2) consists of 6 scalar equations and 12 unknowns (3 components of the resultant hip force $\mathbf{R}$ and 9 unknown muscle tensions $\sigma_i$, $i = 1,2,\ldots,9$). As the number of unknowns of the model exceeds the number of model equations, in general, an infinite number of solutions can satisfy the system. The number of the unknowns was reduced by assuming that the muscle tension of the muscles within the same group (anterior, middle, and posterior, respectively) is equal.[14]

The geometry of the individual hip and pelvis was taken into account by rescaling the reference attachment points and the interhip distance. For that, the values of the hip and pelvic geometrical parameters were measured from the standard anteroposterior rentgenograph of a given patient (Fig. 1A): the interhip distance ($l$), the pelvic height ($H$), the pelvic width ($C$), and the vertical and the horizontal distance from the center of the femoral head to the effective muscle attachment point (T) on the greater trochanter ($z$ and $x$, respectively). The point T is determined by the intersection of the contour of the greater trochanter and the normal through the midpoint of the straight line connecting the most lateral point and the highest point on the greater trochanter. In the one-legged stance, the resultant hip force lies almost in the frontal plane,[13,14] so it is considered that the

component of the force perpendicular to the frontal plane is zero. The resultant hip force is represented by its magnitude $R$ and its inclination with respect to the vertical direction $\vartheta_R$ (Fig. 1B). The medial direction of $\vartheta_R$ is considered as positive.

The values of the components of the resultant hip force are then used to determine the distribution of the contact hip joint stress and the size of the weight-bearing area. Within the model of stress distribution used in this work, it is assumed that when unloaded, the acetabular shell and the femoral head have spherical shape with coincident centers. Upon loading, the intermittent cartilage layer is squeezed. The contact hip stress at any point of the weight-bearing area is assumed to be proportional to strain in the cartilage layer. The point of closest approach of the spherical surfaces of the acetabulum and the femoral head is called the stress pole with the spherical coordinates $\Theta$ and $\Phi$.[12] The above assumptions lead to the cosine dependency of the contact stress distribution in the articular sphere representing the hip joint,[11]

$$p = p_0 \cos\ \gamma \qquad \text{(A1.8)}$$

where $p_0$ is the value of stress at the pole, and $\gamma$ is the angle between the radius vector to the chosen point and the radius vector to the stress pole. The weight-bearing area $S$ is defined as a part of the articular sphere constrained by the acetabular geometry as well as by the position of the stress pole. The lateral border of the weight-bearing area, determined by the acetabular geometry, may be visualized as an intersection of the articular sphere with a plane passing through the center of the sphere and being inclined by the center-edge angle of Wiberg ($\vartheta_{CE}$ ) with respect to the vertical axis. Because only the positive values of stress have a physical meaning, the medial border of the weight-bearing area is determined as the line where stress vanishes ($\cos\ \gamma = 0$). The medial border thus consists of all the points that lie $\pi/2$ away from the stress pole and may likewise be visualized as an intersection of the articular sphere with a plane passing through the center of the sphere, the inclination of this plane being determined by the location of the stress pole. As both intersection planes are passing through the center of the sphere, they both form circles of radii $r$ at the intersection of the plane and the articular sphere. The weight-bearing area is therefore confined by these 2 intersecting circles on the articular sphere.

With known magnitude and direction of **R**, the distribution of the contact stress in the hip joint can be computed from the equation

$$\int_S p\ dS = \mathbf{R} \qquad \text{(A1.9)}$$

where we integrate over the weight-bearing area. Because the resultant hip force lies in the frontal plane, its component perpendicular to this plane is zero, and because the weight-bearing area is symmetric with respect to the direction of the resultant hip force, the 3-dimensional problem can be mapped onto a 2-dimensional one. Thus, the polar angle $\Theta$ determines the angular displacement of the pole from the vertical axis. It is taken that $\Theta$ is positive in the lateral direction. The components of the vector equation (A1.9) yield,[12]

$$\vartheta_R + \Theta \mp \arctan\left(\frac{\cos^2(\vartheta_{CE}-\Theta)}{\pi^{\mp}\left(\frac{\pi}{2}-\vartheta_{CE}+\Theta-\frac{1}{2}\sin(2(\vartheta_{CE}-\Theta))\right)}\right)=0. \qquad \text{(A1.10)}$$

$$p_0 = \frac{3R}{2r^2}\left(\frac{\cos(\vartheta_R+\Theta)}{\pi^{\mp}\left(\frac{\pi}{2}-\vartheta_{CE}+\Theta-\frac{1}{2}\sin(2(\vartheta_{CE}-\Theta))\right)}\right), \qquad \text{(A1.11)}$$

and

$$\Phi = 0 \text{ or } \Phi = \pi. \qquad \text{(A1.12)}$$

Here, the upper sign stands for the case when the pole lies on the lateral side of the contact hemisphere or outside the contact hemisphere in the lateral direction, and the lower sign stands for the case when the pole lies on the medial side of the contact hemisphere or outside the contact hemisphere in the medial direction. The value of $\Theta$ is determined numerically from Eq. (A1.10) using the Newton iteration method and inserted into Eq. (A1.11) to obtain the value of stress at the pole $p_0$. If the pole of stress distribution is located within the weight-bearing area, the location of the peak contact stress ($p_{max}$) coincides with the location of the pole. When the stress pole lies outside the weight-bearing area, the peak contact stress is located at the point on the weight-bearing area, which is closest to the pole. The stress distribution is calculated by using Eq. (A1.8). Figure 1B shows the stress distribution in the frontal plane represented by the shaded area. The extension of the shaded area in the direction perpendicular to the surface of the femoral head indicates the values of stress. The position of the peak stress ($\Theta$) is marked.

## APPENDIX 2: DETERMINATION OF THE SHEAR STRESS IN THE FEMORAL NECK

The femoral neck is considered as a homogeneous beam of circular profile with the diameter 2 (Fig. 1A) clamped to the femoral diaphysis and subjected to bending and compression. The epiphyseal growth plate of the femoral neck forms an angle $\beta$ with respect to the longitudinal axis of the femoral neck (Fig. 1A). It is taken that the beam is free at the side of the femoral head while it is constrained to an imaginary wall (representing the femur) at the other side. The origin of the coordinate system ($\xi,\psi,\zeta$) is placed at the imaginary constraining point to the femur (Fig. 1B). The loading force $\boldsymbol{R}$ (lying in the frontal plane) was decomposed into 2 components: the compressive component parallel to the longitudinal axis of the neck ($\xi$) $P = R\sin(\vartheta_R + \vartheta_{CCD} - 90°)$ and the shear component perpendicular to the longitudinal axis of the femoral neck ($\psi$) $F_S = R\cos(\vartheta_R + \vartheta_{CCD} - 90°)$ where $\vartheta_R$ is the inclination of the force $\boldsymbol{R}$ from the vertical axis and $\vartheta_{CCD}$ is the CCD (caput-collum-diaphysis) angle (Fig. 1). The component $P$ compresses

the bone, whereas the component $F_S$ induces shear stress and bending of the femoral neck. The stress acting within the plane perpendicular to the longitudinal axis of the neck can be described by assigning to each point the elements of the stress tensor,

$$\sigma_p \begin{bmatrix} \sigma_\xi & \tau \\ \tau & 0 \end{bmatrix}, \qquad \text{(A2.1)}$$

where $\sigma_\xi = -4P/\pi a^2 + 64F_s\psi(\xi-\xi_R)/\pi a^4$ is the compressive stress, $\xi_R$ is the coordinate of the origin of the force **R** and $\tau$ is the shear stress.[31]

$$\tau = 64F_s\left((a^2/4-\psi^2)^2+\psi^2\zeta^2\right)^{1/2}/3\ \pi a^4 . \qquad \text{(A2.2)}$$

It follows form the above that the bending of the femoral neck induces nonuniform shear stress $\tau$, which reaches a peak value

$$\tau_0 = 16F_s/3\pi a^2 , \qquad \text{(A2.3)}$$

at the center of the neck cross section.

Because the epiphyseal growth plate of the femoral neck forms an angle $\beta$ with respect to the longitudinal axis of the femoral shaft (Fig. 1A), we were interested to calculate the elements of the tensor $\sigma_P$ in the plane defined by the epiphyseal growth plate. For that, the coordinate system should be rotated for an angle $\omega$,

$$\underline{\sigma}_{P\beta} = \underline{R}^{-1}\underline{\sigma}_P\underline{R} , \qquad \text{(A2.4)}$$

where $\underline{R}$ is the rotation matrix,

$$\underline{R} \equiv \begin{bmatrix} \cos\omega & \sin\omega \\ -\sin\omega & \cos\omega \end{bmatrix}, \qquad \text{(A2.5)}$$

with $\omega = (\vartheta_{CCD} - \beta - 90°)$. The peak shear stress in the oblique plane of the epiphyseal cartilage (at $\psi = 0$) $\tau_{0\beta}$ is therefore

$$\tau_{0\beta} = -2R\cos(\vartheta_R + \vartheta_{CCD})\sin(2\omega)/(\pi a^2) - 16R\sin(\vartheta_R + \vartheta_{CCD})\cos(2\omega)/(3\pi a^2). \qquad \text{(A2.5)}$$

To determine the peak shear stress $\tau_{0\beta}$, the geometrical parameters $\vartheta_{CCD}$, $\beta$, and $a$ (Fig. 1A) were measured from standard anteroposterior radiograms. The magnitude and direction of the resultant hip force ($R$ and $\vartheta_R$, respectively) were calculated by the HIPSTRESS method as described in Appendix 1.